PCCP

PAPER

Cite this: *Phys. Chem. Chem. Phys.*, 2023, **25**, 3834

Computer simulation of obtaining thin films of silicon carbide†

Alexander Y. Galashev *[ab] and Ksenia A. Abramova [ab]

Silicon carbide films are potential candidates for the development of microsystems with harsh environmental conditions. In this work, the production of high-purity silicon carbide films by the electrolytic method is reproduced in a computer model. Single-layer SiC films were deposited on nickel, copper, and graphite substrates. The kinetic and structural characteristics related to the Si and C atoms in this compound are presented. The coefficient of self-diffusion of C atoms on all substrates is higher than that of Si atoms. In addition, the diffusion of atoms on a graphite substrate occurs much more intensively than on metallic (Ni and Cu) substrates. The first maximum of the radial distribution function $g(r)_{SiC}$ is at a shorter distance when the film is deposited on the graphite substrate. A detailed analysis of the structure, based on the construction of Voronoi polyhedra, indicates that the degree of crystallinity of the film increases when changing the substrate in the order from nickel to graphite. The resulting SiC films are subject to local stresses, the strongest of which appear on the copper substrate, however the average stresses in the film do not appear to be high.

Received 9th September 2022,
Accepted 9th January 2023

DOI: 10.1039/d2cp04208h

rsc.li/pccp

1. Introduction

Thin film silicon carbide has characteristics that make this material suitable for use in microelectronics (diodes, thin film transistors, blue or multicolor LEDs), electrochemical devices and microelectromechanical systems.[1] Due to good thermal and electrical conductivity, as well as high mechanical strength, silicon carbide films can be used as the basis for composite materials used in opto- and microelectronics. For example, in ref. 2, the possibility of using SiC thin films to stabilize two-dimensional stanene is shown; such a hybrid can be used in the development of next-generation topological transistors, quantum computers, and superconductors. However, the efficiency of thin-film devices is highly dependent on their structural, electrical, mechanical, and optical properties The work[3] shows the effect of various vacancies on the thermal conductivity of the material, it was found that the presence of 1% defects in the material leads to a decrease in heat transfer properties by about 2 times. Thin film silicon carbide can replace a similar silicon material when used in harsh environments such as high temperatures and high levels of radiation. Among the electronic properties of silicon carbide, one can single out a wide band gap, a high electron saturation rate, and a large breakdown field.[4] Silicon carbide can serve as a protective coating in heat exchangers.[5] This is facilitated by its low coefficient of thermal expansion, low neutron absorption cross section, high thermal conductivity, high hardness and excellent tribological, chemical and oxidation resistance. In addition, SiC coatings are suitable for biomedical applications,[6] passivating coatings on metallic materials,[7] and as barrier layers for solar cells.[8] Films of hydrogenated amorphous silicon carbide (a-SiC:H) can be used in optoelectronic devices,[9] solar cells,[10] and also as high-temperature coatings[11] and X-ray masks.[12] Among other things, SiC can be used to obtain graphene. In work[13] discusses the method of thermal graphitization of silicon for the controlled production of graphene layers. With this approach, silicon atoms evaporate from the SiC surface at temperatures above 1000 K, and the remaining carbon atoms form epitaxial graphene. The type and concentration of defects in the initial silicon carbide have a significant effect on the physical properties of the resulting graphene. Defect engineering makes it possible to control the distribution of defects in a material and thus influence the magnetic properties of a material.[14,15]

Thin SiC films can be obtained by various methods, and the structure of the film depends on the method of its preparation. For example, crystalline films can be obtained using pulsed laser deposition, while the sputtering DC magnetron method makes it possible to obtain amorphous SiC films.[16] The method of combined use of DC magnetron sputtering and high-power pulsed magnetron sputtering makes it possible to deposit almost stoichiometric and nanocrystalline SiC thin films at

[a] *Institute of High-Temperature Electrochemistry, Ural Branch of Russian Academy of Sciences, Academicheskaya Str., 20, Yekaterinburg 620137, Russia. E-mail: galashev@ihte.uran.ru*

[b] *Ural Federal University named after the first President of Russia B.N. Yeltsin Mira Str., 19, Yekaterinburg 620002, Russia*

† Electronic supplementary information (ESI) available. See DOI: https://doi.org/10.1039/d2cp04208h

 This journal is © the Owner Societies 2023

room temperature on silicon (100) substrates.[17] The hardness of the resulting coating and its Young's modulus significantly depend on the pressure of the atomizing gas. Thin crystalline SiC films of good quality can be produced by fast thermal chemical vapor deposition.[18] To do this, carbonization of Si substrates is carried out using a hot-wall reactor, which creates fast thermal chemical vapor deposition. To obtain SiC films, ion sputtering, electrochemical deposition from molten salt, and the sol–gel method are also used.[19] These methods are not used as often due to the complexity of the experiment, including high vacuum and high temperature. However, the liquid deposition method has a number of advantages, such as the availability for large area deposition on intricate surfaces, low power consumption, and ease of setup compared to vapor deposition methods. Lowering the deposition temperature can lead to the formation of crystalline grains, which are undesirable in the film structure. Iodine, which has a lower electronegativity and oxidizing properties, as well as a larger atomic mass and radius (than F and Cl), reduces reactivity in high-temperature exchange reactions. Therefore, it is more probable that during the co-precipitation of Si and C from the KF–KCl–KI ternary melt, a uniform distribution of carbon and silicon atoms in the resulting film will be achieved.

Fabrication of thin films by electrolytic deposition is one of the cheapest methods for obtaining two-dimensional materials with precisely controlled composition. The composition of the electrolyte has a significant effect on the quality of the resulting films. Therefore, the selection of an electrolyte is very important to perform a given electrodeposition. In particular, one of the promising electrolytes is the KF–KCl–KI ternary melt, which can be used to obtain both high-purity silicon and precision compounds of silicon and graphite, hydrogen, and other elements. Considerable attention is paid to the study of the physicochemical properties of such a melt.

An experimental study of the viscosity of the KF–KCl–K_2SiF_6 melt containing two of the three components of the melt chosen by us for obtaining SiC films showed that the melt (KF–KCl)eut.-(10 mol%) K_2SiF_6 at temperatures below 898 K is in the form suspension, and its homogeneity extends to the temperature range 903–993 K.[20] A melt with identical (*i.e.*, chosen by us) components was used to study the electrodeposition of silicon on a glassy carbon electrode using cyclic voltamperometry, chronamperometry, and scanning electron microscopy.[21] It was found that an increase in the concentration of KI leads to the formation of denser silicon deposits. For the KF–KCl–KI system, the eutectic composition with mol%: 25 – KF, 34 – KCl, 41 – KI, having a melting point of 750 K was established by the method of synchronous thermal analysis.[22] The temperature dependences of the densities of melts with mol%: 45 – KF, 55 – KCl, KI and 66.6 – KF, 33.4 – KCl, KI with a KI content from 0 to 100% are described by linear functions in the temperature range of 973–1073 K.[23] An electrolyte close to ours (17% KCl, 8% KF, 75% KI) was used in the electroreduction of silicon on a copper substrate by cyclic voltammetry at 993 K.[24] A uniform distribution of the dopant (p- or n-type) was demonstrated using the co-deposition method.[25]

The structure has a great influence on the physical properties of materials. Computer simulation allows a detailed structural analysis. For example, in ref. 26, the Monte Carlo method was used to study the structural development of amorphous and nanoporous carbon, silicon, and silicon carbide. In,[27,28] thin films of pure silicon were obtained by molecular dynamics modeling of electrodeposition from KF–KCl–KI melt. A detailed structural analysis of the obtained films was performed.

It should be noted that during the electrolytic synthesis of materials, it is possible to form multilayer composite coatings; in this case, the key factor is the choice of the substrate. Of interest is the study of interaction with substrates that meet the following requirements: low ability of the obtained films to form alloys with the substrate surface, good conductivity, the economic benefit of the scientific and technical use of the obtained composites. In this regard, we considered nickel, copper, and graphite substrates.

The graphite substrate was taken as the main one for comparison with the results of SiC film deposition on metal (Cu and Ni) substrates. The point is that the beta-SiC was grown on graphite by chemical vapor deposition (CVD) at relatively high deposition temperatures (1473–1673 K) using SiCl4, C_3H_8, and H_2 gas mixtures.[29] Well-ordered graphite films of nanometer thickness were obtained on a Ni substrate.[30] Single-layer graphene on Cu was grown by CVD in a CH_4/H_2 reactive atmosphere at 1250–1350 K, although from the point of view of thermodynamics, the growth of multilayer graphene is more favorable.[31] For the deposition of SiC, transition metal substrates were chosen, which, for example, for CVD of graphene act as a catalyst accelerating the reaction without wasting the substrate material. Copper, unlike nickel, has a weak catalytic activity. Graphene grows on Cu, which has a lower carbon solubility, mainly through surface reaction, which usually gives a few layer graphene. The growth of graphene on Ni, which has a significantly higher solubility of carbon, proceeds by carbon segregation/precipitation during cooling (resulting in single layer graphene). At relatively low temperatures (up to 800 K), Cu and Ni are practically insoluble in silicon.[32] Based on the available literature data, it is not possible to predict the mechanism of growth of silicon carbide films in a salt melt on Cu and Ni surfaces.

A different pattern of film growth on the surface can also be observed at different direction of the substrate to the melt–substrate interface. In the work,[33] where 3C–SiC epitaxial films were grown on Si(111) and Si(100) substrates by the atom substitution method. The formation of silicon carbide occurred by means of the substitution of a portion of Si atoms by C atoms as a result of a chemical reaction

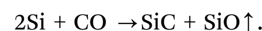

$$2Si + CO \rightarrow SiC + SiO\uparrow.$$

As a result, in both cases, as a rule, polycrystalline SiC films with a grain size of $\sim$27.5 nm were obtained. Note that epitaxial growth occurred in the [001] direction if Si(001) served as the substrate surface. Predominantly the same direction was perpendicular to the surface of the formed film in the case of using the Si(111) substrate. In the opinion of the authors, in

both cases, the film growth occurred in the presence of local stresses. We chose substrates with a front (facing the melt) crystallographic surface (001) in the expectation that multilayer SiC films (which we expect to obtain in the future) will grow in the direction determined by the substrate, *i.e.* [001]. In this case, one can expect to obtain a thicker film than a single layer film, with a cubic three-dimensional structure, which will facilitate its identification.

In this work by computer simulation, an electrochemical route to deposit silicon–carbon films using a KCl (19.2 mol%) – KF (9.6 mol%) – KI (71.2 mol%) melt at atmospheric pressure and temperature 1000 K has been developed. This study expands the search for opportunities to obtain large-area high-purity SiC films and reveals at the atomic level the structural features of films deposited on metal and non-metal surfaces.

2. Computational details

2.1 System formation

To prepare the initial system representing a molten salt, three crystals (KCl, KF, KI – fcc lattice) were placed above the substrate (Cu(001), Ni(001) or graphite). The crystals of the melt components were at a distance of $r \approx 0.4$ nm from each other and from the substrate (Fig. 1). The metal substrates were represented by four layers of the fcc crystal lattice. The densities of nickel and copper crystals were 8.9 and 8.94 g cm^{-3}, respectively. A nickel or copper substrate in the form of a crystalline plate was facing the melt with the (001) plane. The graphite substrate included 4 layers of graphene, which were arranged one above the other in accordance with the ABAB stacking. The distance between the layers was 0.335 nm. In the cases of Ni, Cu, and a graphite substrate, the systems prepared for the deposition of Si and C atoms contained 13788, 13797, and 15769 atoms, respectively. The number of atoms forming the melt was the same for all systems: 1728 KCl atoms (19.2 mol%), 864 KF atoms (9.6 mol%), 6400 KI atoms (71.2 mol%). The system had dimensions: 7.68 × 7.68 × 11.7 nm. The interaction between the melt components was described by a potential including the Coulomb and Lennard-Jones (LJ) parts:

$$\Phi(r_{ij}) = \frac{Z_i Z_j}{r_{ij}} + 4\varepsilon\left[\left(\frac{\sigma}{r_{ij}}\right)^{12} - \left(\frac{\sigma}{r_{ij}}\right)^{6}\right], \quad (1)$$

where Z_i-charge of i-ion, $r_{ij} = |r_i - r_j|$ distance between i–j ions, ε-potential well depth, σ-distance when the LJ interaction between i–j ions is vanishes.

The Lennard-Jones potential is not universal and poorly describes solid–solid interactions. Therefore, in the present model, the interaction of silicon with substrate surfaces was described by the Morse pair potential.[34] The interaction between deposited Si, C atoms and graphite substrate was described by the Tersoff potential.[35] The parameters for all presented potentials are given in the Appendix A. The served to simulate the electrolyte-surface interface, the substrate atoms were immobile; therefore, the potential describing the interaction of deposited atoms with the substrate was not specified.

After the equilibrium melt was prepared, the Si and C deposition simulation onto the substrate began.

2.2 Heating and melting

Periodic boundary conditions (PBCs) acted in (x, y) direction, and fixed boundary conditions (FBCs) acted in the z direction. The step of integrating the equations of motion was 1 fs. Before starting molecular dynamics (MD) modeling, a geometric optimization procedure was performed. This procedure (minimization) was carried out by the Polack–Ribière conjugate gradient method.[36] The melting of the entire system was realized within 1.4 ns in the temperature range 0–1750 K (Fig. 1). As a result, the mixing of all components of the melt was achieved. The melting of the system was fixed by partial radial distribution

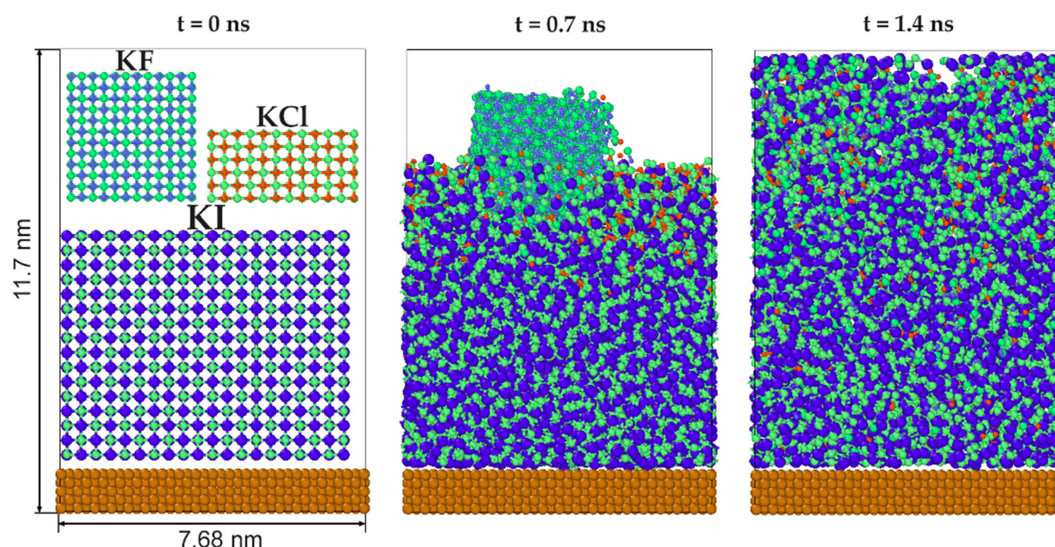

Fig. 1 Melting stages of KF, KCl, KI crystals with the achievement of complete mixing of the melt at a temperature of 1750 K.

This journal is © the Owner Societies 2023

functions analysis of the melt components and melt structure detailed analysis by constructing Voronoi polyhedra. Fig. 1 shows the chronology of obtaining an equilibrium KF–KCl–KI melt during modeling in the *NVT* ensemble. It can be noted that at the final stage of relaxation, the melt components are well mixed. Then the system was relaxed in the *NPT* ensemble within 0.5 ns to reach the experimental density value $\rho \approx 1.9$ g cm^{-3}.[23] The main simulation (deposition of Si and C particles) was performed in the *NVT* ensemble at a temperature of 1000 K.

2.3 Deposition process

The deposition of Si^{4+} and C^{4+} ions was carried out in the KF–KCl–KI melt after obtaining a stable melt-substrate interface. To simulate the electrolysis process, a constant electric field with a strength of $E = 10^4$ V m^{-1} was introduced. This electric field acted only on the Si and C ions, and created an additional vertical force directed towards the substrate. The deposition process schematically presented in the Fig. 2. The deposition was carried out by periodic alternate introduction of Si^{4+} and C^{4+} ions. Ions had random x, y coordinates and a fixed coordinate $z = 11$ nm. Thus, ions were randomly distributed on the substrate surface, and the path of ions through the melt medium to the final site on the substrate was determined only by the density of the melt and the parameters of interaction with the substrate. New silicon and carbon ions appeared in a certain region of the system every 30 and 50 ps, respectively. The time of 30 ps for the appearance of a new Si^{4+} ion was chosen empirically when simulating the electrolytic deposition of silicon on silver and graphite substrates.[27] As a rule, at least 2/3 of this time the Si^{4+} ion spent on the passage of the melt, and the rest of the time was spent on finding a settled place on the substrate. The time of appearance of a new C^{4+} ion in the system was also selected empirically: firstly, the computer time of one calculation should be minimal; secondly, the Si^{4+} and C^{4+} ions should not be associated in the melt, forming clusters in the melt, which hindered the formation of a silicon carbide film on the surface. Based on these requirements, the optimal time for the appearance of C^{4+} ions in the melt (50 ps) was determined for this model. In practice, the SiC film is deposited on the cathode; negatively charged electrode. Therefore, upon reaching this electrode, a positively charged Si^{4+} or C^{4+} ion acquires the missing electrons and becomes an electrically neutral atom. In the model under consideration, the lifetime of Si^{4+} and C^{4+} ions are limited to 30 and 50 ps, respectively. The rest of the time, these particles spend as atoms, which are no longer affected by the electric field. The total deposition time for each type of substrate was approximately 78 ns. The deposition process was completed when a single layer coating on the metal substrates was basically obtained and the number of atoms deposited on the graphite substrate was approximately equal to the number of atoms deposited on each of the metal substrates. The initial velocity of Si^{4+} or C^{4+} ions had a nonzero value only for the z component, which was -0.01 nm ps^{-1} (the "$-$" sign reflects the direction of the velocity vector).

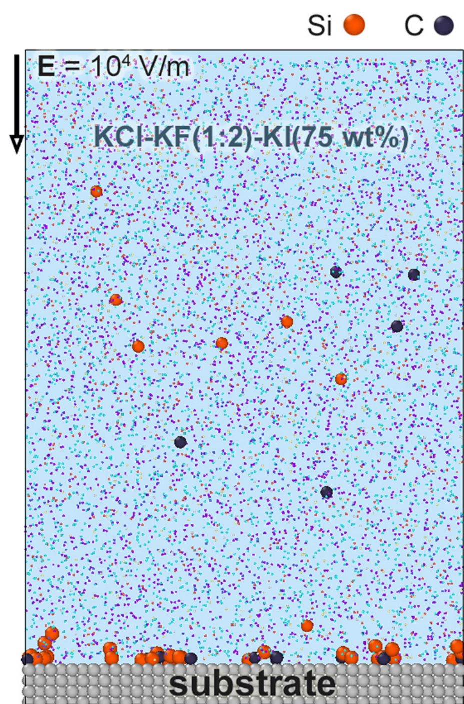

Fig. 2 Schematic representation of the Si^{4+} and C^{4+} deposition process from the melt to the substrate. Ions were introduced in the system periodically, the particles moved through the melt in the substrate direction under the action of the electrical field **E**.

After the process of deposition was completed (the introduction of new particles into the system was stopped), the final relaxation was performed within 1 ns (*NVT* ensemble). At this stage, based on the construction of Voronoi polyhedra (VP), the detailed structure of the obtained films was studied.

2.4 Surface diffusion and mechanical stresses study

To determine the influence degree of the substrate on the formed SiC films, as well as to determine the differences in the mechanisms of formation of such films, we calculated the surface diffusion coefficients for the Si and C atoms located on the substrate. The Si or C particle coming from the melt was considered to belong to the substrate if its distance to the substrates, determined along the normal to the surface, did not exceed 2 $L_{\text{Si-X}}$, where $L_{\text{Si-X}}$ is the bond length between Si and Ni, Cu or C atoms, which has the values 0.24, 0.26 and 0.20 nm, respectively.[37,38] The diffusion coefficient was calculated according to the formula:

$$D = \frac{1}{2\Gamma N} \lim_{t \to \infty} \frac{1}{t} \left\langle \sum_{i=1}^{N} (\Delta \mathbf{r}_i)^2 \right\rangle, \qquad (2)$$

where for three-dimensional space $\Gamma = 3$, N is the number of particles in the system, t is the time of observation of the displacement of atoms at a certain initial time t_0, $\Delta\mathbf{r}_i(t) = \mathbf{r}_i(t) - \mathbf{r}_i(t_0)$ is the displacement of the i atom relative to the position that it occupied at the initial time instant t_0, summation is performed over all N particles of the system, $\langle \ldots \rangle$ denotes averaging over the initial times used to determine D.

To determine the stress state of the films, we calculated the stress tensor for these thin layers. The entire film was divided

into L strips. The film surface was subdivided both in the direction of the $0x$ axis and in the direction of the $0y$ axis. The calculation of the $\sigma_{\gamma\alpha}(l)$ stress appearing on the elementary area with the number l was determined by dividing the resulting force by its area S_l. The resulting force was determined as the sum of the vectors of all interatomic forces passing through the area.[39] When determining the $\sigma_{\gamma\alpha}(l)$ value, the interaction was taken into account both between solely film atoms and between the film and substrate atoms. Index γ shows the direction of the site orientation, and the index $\alpha = (x, y, z)$ indicates the direction of action of the resulting force component.

Thus, the stress at an elementary site can be calculated according to the expression:

$$\sigma_{\gamma\alpha}(l) = \left\langle \sum_i^n \frac{1}{\Omega}\left(mv_\gamma^i v_\alpha^i\right) \right\rangle + \frac{1}{S_I}\left\langle \sum_i^n \sum_{j\neq i}^{(u_i\leq u, u_j\geq u)} \left(f_{ij}^\alpha\right) \right\rangle, \quad (3)$$

where n is the number of atoms on the l area, m is the atomic mass, v_α^i is the α projection of the velocity of the i atom, Ω is the volume per atom, f_{ij}^α is the α projection of the resulting force from the interaction between i and j atoms that passes though the l area, and u_i is the coordinate of the atom i; the coordinate of the contact point of the straight line passing through the centers of the atoms i and j and the l surface element is denoted through the symbol u.

3. Result

Fig. 3 shows the structures obtained on nickel, copper, and graphite substrates at the final stage of MD simulation. The difference in the "substrate-SiC" interaction leads to the different coating formation mechanisms. The film on the metal surface is formed predominantly layer-by-layer, *i.e.* the formation of the second SiC-layer occurs after the majority of the metal surface is covered. In the case of a graphite surface, the subsequent layers of the SiC film growth begins much earlier, in other words, three-dimensional growth in this case competes strongly with layer-by-layer growth. Fig. 4 shows the stages of growth of silicon carbide films on graphite and nickel. It can be noted that in the case of a metal substrate, several islands are formed on the surface, expanded as new Si and C particles enter the system. On the graphite substrate, it can be seen, an active and mobile growth center is formed, which attaches Si and C particles from the melt. As a result, a cluster weakly bound to the substrate is formed on the surface. In this case, a significant part of the substrate remains uncovered.

To estimate the kinetic properties of silicon and carbon surface particles, as well as to determine the effect of the substrate on the film formation mechanism, the surface self-diffusion coefficients D for Si and C particles were calculated. Fig. 5 shows the dependencies of D on the number of the deposited atoms (N_{atoms}) for all surfaces. It can be noted that the average D values calculated for metal surfaces turn out to be approximately the same ($2.5\text{–}3 \times 10^{-8}$ cm^2 s^{-1}). In both cases, the maximum value of the self-diffusion coefficient is reached at the initial stage of deposition at $N_{\text{atoms}} < 600$ and is 6.2×10^{-8} cm^2 s^{-1} (for C) and 4.5×10^{-8} cm^2 s^{-1} (for Si). As the substrate surface is filled, D decreases significantly, and with a total number of deposited particles $N_{\text{atoms}} > 1000$, the value of D drops to $10^{-10}\text{–}10^{-12}$ cm^2 s^{-1}. It can also be noted that, in all cases, C atoms are more mobile than Si atoms, which is explained by the small size of the carbon particle, as well as the weaker C–C bond than the Si–C bond.[40] For a nickel substrate, the difference between the D coefficients is approximately 30%, for a copper substrate, 20%.

In the case of a graphite substrate, the value of D is higher on several orders and amounts $\sim 10^{-6}$ cm^2 s^{-1}, this reduces the probability of Si and C particles being on the substrate, thereby facilitating sp^3 hybridization and, as a consequence, the formation of a single active SiC cluster on the surface. However, at the size cluster size of 2.5×7 nm, *i.e.*, in the case when 32% of

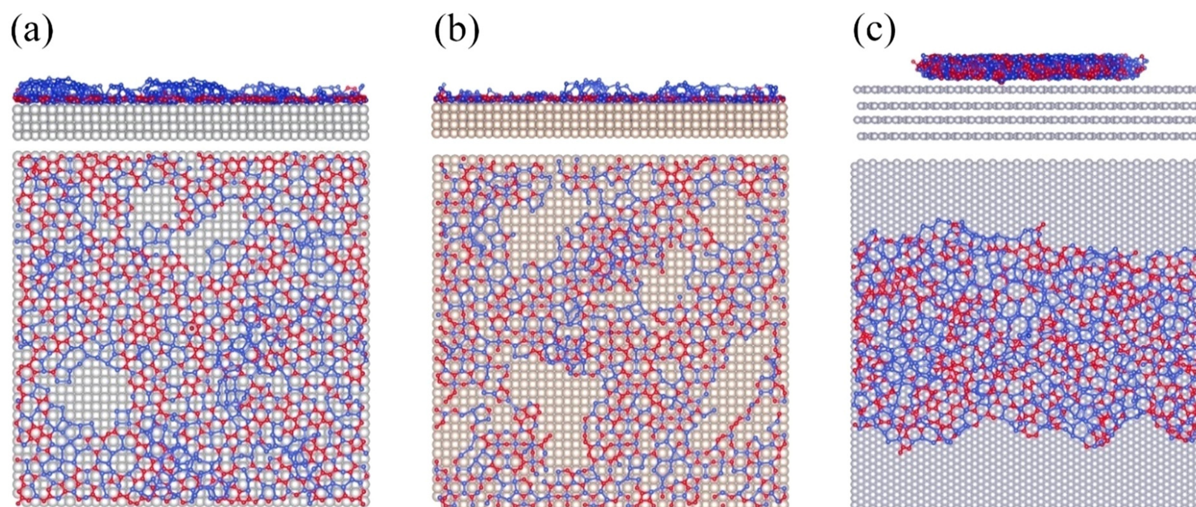

Fig. 3 *xy*-projections of deposited SiC films on (a) nickel, (b) copper, (c) graphite substrates. In the case of metal substrates, the simulation time is ≈60 ns, in the case of graphite, ≈50 ns. Carbon atoms are marked in red; silicon atoms are marked in blue.

 This journal is © the Owner Societies 2023

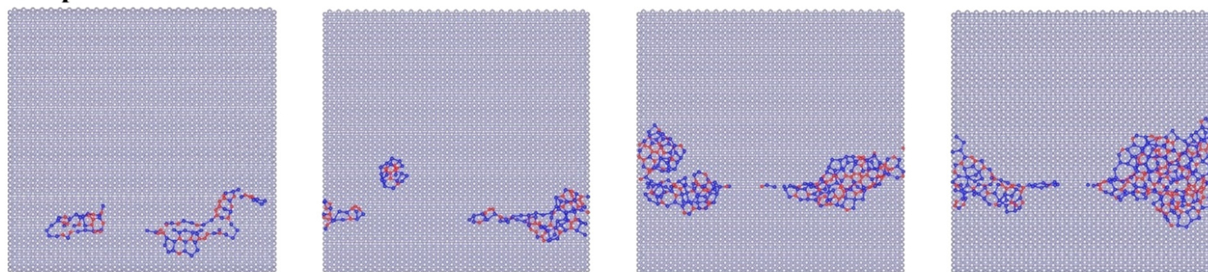

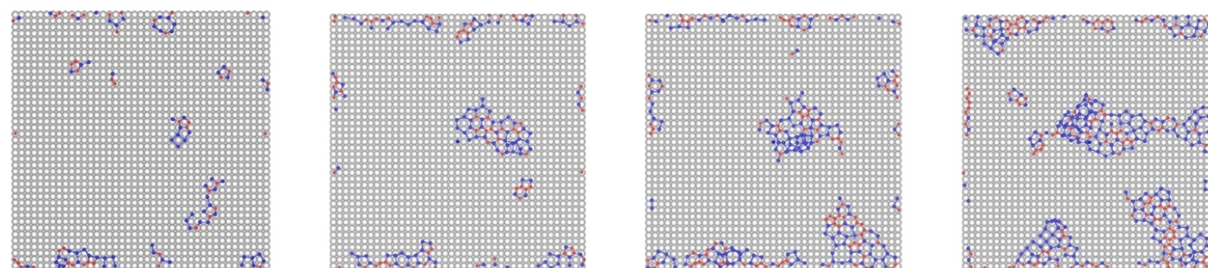

Fig. 4 Stages of growth of SiC films on graphite (top) and nickel (bottom). C atoms are marked in red; Si atoms are marked in blue.

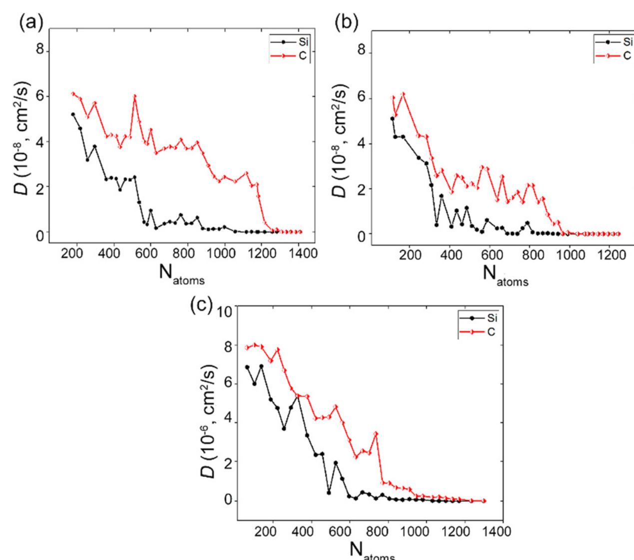

Fig. 5 The surface diffusion D of Si (in red) and C (in black) depending on the total number of atoms on the Ni(001) (a), Cu(001) (b), graphite (c) substrates.

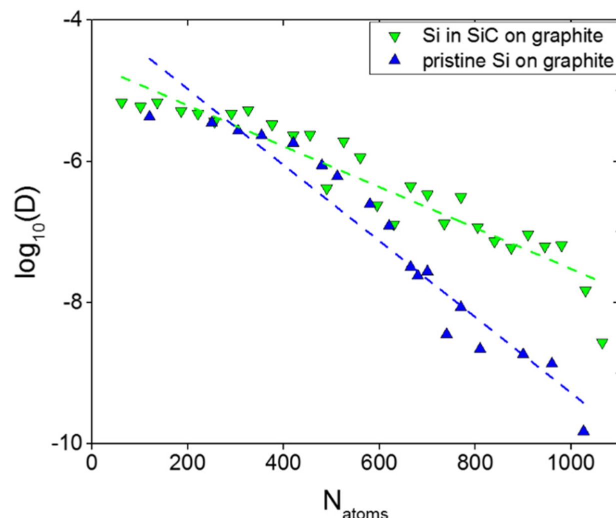

Fig. 6 The surface diffusion (on a logarithmic scale) dependent on the number of particles deposited on a graphite substrate. The system with only Si-atoms marked in blue, the system with silicon and carbon atoms – in green. The dashed-dotted line shows a linear approximation.

the substrate area is covered by the film ($N_{\text{atoms}} > 800$), the cluster mobility sharply decreases.

Fig. 6 shows the surface diffusion of silicon during deposition on graphite (in blue). For comparison, the $\log_{10}D(N_{\text{atoms}})$ dependence found in ref. 26 for the deposition of pure silicon is presented (in green). The dashed-dotted lines show the linear approximation. At the initial stage, the surface mobility of Si atoms turns out to be 4.29×10^{-6} cm^2 s^{-1} in the case of deposition of pure silicon and 6.89×10^{-6} cm^2 s^{-1} for silicon in a system where carbon was also present. At $N_{\text{atoms}} < 500$, the dependencies correlate; when the number of the surface particles increased, the dependence for pure silicon becomes steeper, which corresponds to a rapid decrease in the value of surface diffusion. In the case of the presence of carbon in the system, the dependence decreases more slowly, since three-dimensional growth begins before the film covers the entire surface of the substrate (Fig. 3).

The partial radial distribution functions $g(r)_{\text{Si–C}}$ were calculated at the final stage of modeling for 1 ns ($1\,000\,000\Delta t$) at 1000 K, when the new Si and C particles do not enter the system

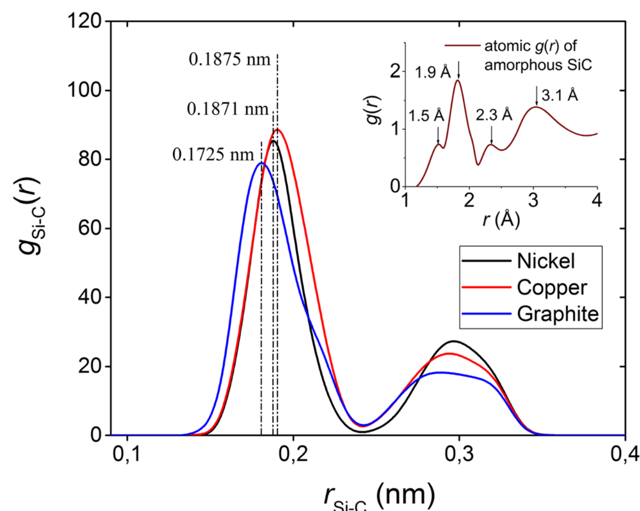

Fig. 7 Radial distribution function of Si–C for various substrates, at the stage of final relaxation, when new particles did not enter the system. The figure shows the Si–C distances corresponding to the main peaks of the function at the temperature T = 1000 K; in insert: atomic pair-distribution function, $g(r)$, of amorphous SiC induced by ion-beam irradiation;[42] arrows show peak and sub-peak locations.

(Fig. 7). Let us compare the locations of the first peaks r_{Si-C} of this function with the lengths Si–C bonds (l_{Si-C}). It was shown in ref. 41 that the average Si–C bond length in crystalline silicon carbide at a temperature of 900–1000 K is 0.18 nm. The calculated first peak location of the SiC on metal substrates is at 0.187 nm, *i.e.* in this case, the Si–C bond on the substrate is stretched by ~4% compared to l_{Si-C} of bulk SiC. At the same time, when the film is on the graphite surface, the first peak is localized at 0.17 nm; the most probable distance between Si and C atoms determined in this way turns out to be 6% shorter than the Si–C bond length in silicon carbide. The bond length change in the SiC film on the different substrates correlates with the nearest distances (Ni–Ni, Cu–Cu and C–C) between atoms in the respective substrates. These distances in Ni (r_{Ni} = 0.249 nm) and Cu (r_{Cu} = 0.255 nm) crystals are larger than Si–C bonds (l_{Si-C}) in silicon carbide, and the corresponding distance between C atoms in graphite (r_C = 0.142 nm) is less than l_{Si-C} by ion-beam irradiation;[42] arrows show peak and sub-peak locations.

The inset shows the radial distribution function of all atoms of amorphous SiC obtained by elastic scattering of an electron beam.[42] Heteronuclear bonds Si–C create the main peaks (at 1.9 and 3.1 Å) of the atomic function $g(r)$. In addition, this function has subpeaks associated with homonuclear C–C and Si–Si bonds at 1.5 and 2.3 Å, respectively. The partial function $g_{Si-C}(r)$ obtained for a SiC film on metal (Ni and Cu) substrates has peaks whose locations are close to the locations of the peaks of atomic $g(r)$ generated due to heteronuclear bonds. However, in the case of a graphite substrate, the deviation in the location of these peaks for the experimental and calculated functions is more significant. In other words, the packing of atoms obtained on a graphite substrate differs more strongly from amorphous one than the packing on metal substrates.

The construction of Voronoi polyhedra allows one to study the short-range order in the arrangement of atoms in the form of statistical distributions of VP over the number of faces, faces over the number of sides, or in the form of the distribution of angles formed by pairs of geometric neighbors with a central atom (VP center). These distributions together give an idea of the spatial (3-dimensional) structure of atomic packings, which cannot be obtained using a one-dimensional radial distribution function. In Fig. 8–11 n and m distributions for the carbon and silicon subsystems of SiC films obtained on nickel, copper, and graphite substrates are compared with each other. Also, for comparison, the corresponding distributions for the bulk phase of 4H-SiC modification of silicon carbide are given. The following explanation is appropriate here. To date, more than 250 silicon carbide polymorphs have been identified.[43] The structural, elastic, and electronic properties of 2H-SiC and 4H-SiC polytopes have been studied more carefully. It is these polytopes that have the most favorable structural, elastic, and electronic behavior. The structure of 2H-SiC has a direct analogy to the wurtzite structure. It consists only of elements A and B, stacked in the form ABABAB. The 4H-SiC structure has a twofold longer stacking period for elements A and B, the second half of which differs from the stacking of 2H-SiC. This difference is expressed in the twisting of the elements, so that the ABCB stack is formed in 4H-SiC.[43] The total energy of the 4H-SiC modification is slightly lower than the corresponding 2H-SiC modification; 4H-SiC structure is more stable.

As can be seen from Fig. 8, depending on the type of substrate used, significantly different distributions of VP over the number of faces were obtained. Even the locations of the maxima of these distributions differ from each other. For the nickel, copper, and graphite substrates, the maxima of the n distributions obtained for the carbon subsystem of the SiC film fall at n_m = 6, 7, and 5, respectively. The n distributions themselves in the cases of Ni, Cu, and the graphite substrate extend to n = 11, 13, and 9, respectively. These differences

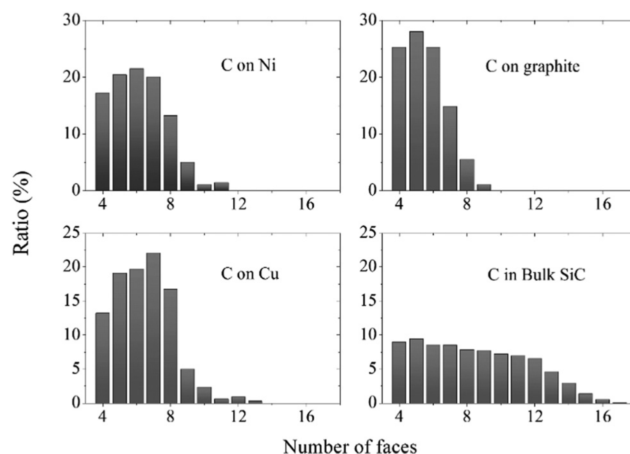

Fig. 8 Distribution of Voronoi polyhedra by the number of faces built for C atoms of SiC films obtained on nickel, graphite, and copper substrate, in comparison with the corresponding distribution for the carbon subsystem of the 4H-SiC bulk phase of silicon carbide modification.

This journal is © the Owner Societies 2023

indicate the different nature of the short-range order in the arrangement of C atoms relative to each other on different substrates. Note that each of these distributions also differs greatly from the corresponding n distribution calculated for the bulk phase of 4H-SiC of silicon carbide modification. The latter distribution is strongly extended, extending up to n = 16, and has a weakly pronounced maximum at n_m = 5. This indicates a significant disorder of C atoms relative to each other in the bulk phase of the SiC modification under study. At the same time, C atoms in a film on a graphite substrate have the highest mutual ordering.

Fig. 9 shows the n distributions for the Si subsystem, similar to the n distributions for the C subsystem presented in Fig. 8. In all considered cases, the n distributions for the Si subsystem are less representative than those for the C subsystem. In other words, the n distributions for the Si subsystem contain fewer face types than the corresponding n distributions for the C subsystem. This indicates a higher mutual ordering of Si atoms on the substrates under consideration and in the bulk 4H-SiC modification of silicon carbide. Just as in the case of n distributions for the C subsystem, there are no equal lengths of n distributions for the Si subsystem. However, it should be noted that the maxima of the n distributions for the Si subsystems of all three films (obtained on different substrates) fall on the same value n_m = 5. At the same time, the maximum of the corresponding distribution for the bulk SiC phase falls on n_m = 4.

The distributions of VP faces over the number of sides or m distributions constructed for the C subsystem of the resulting SiC films and for the 4H-SiC bulk phase of the silicon carbide modification do not look as diverse as corresponding n distributions for this subsystem (Fig. 10). The maxima of the m distributions for the C subsystem of all obtained SiC films fall at m_m = 4, and the maximum of the corresponding m distribution for the bulk SiC phase, at m_m = 5. The dominance of quadrangular faces is a sign of the crystal packing of the considered atoms. The main difference in the m distributions revealed for the C subsystem of films is the different ratio between the number of triangular and pentagonal faces. In the film obtained on a Ni substrate, the proportion of triangular faces (25.4%) is slightly higher than the proportion of the pentagonal faces (23.0%). At the same time, in films on a Cu substrate, an inverse relationship is observed, *i.e.* the number of the pentagonal faces slightly dominates (by 1.9%). A much stronger difference in this feature from the cases with metal substrates is observed in the film obtained on graphite. Here, the proportion of triangular faces (31.9%) significantly exceeds the proportion of the pentagonal faces (21.6%). The lowest proportion of triangular faces in the m distributions shown in Fig. 10 is observed for the bulk SiC phase (12.3%), in the corresponding distribution of which the proportion of the pentagonal faces (31.3%) is only slightly higher than the proportion of quadrangular faces (29.5%).

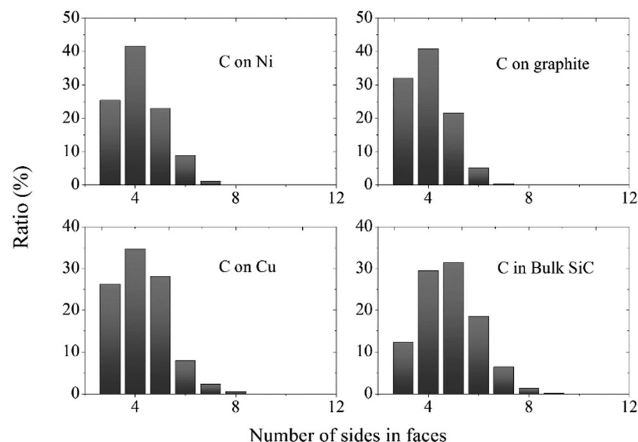

Fig. 10 The distribution of the faces of the Voronoi polyhedrons by the number of sides for the C subsystem of SiC films obtained on nickel, graphite, and copper substrate in comparison with the corresponding distribution for the carbon subsystem of the 4H-SiC bulk phase of silicon carbide modification.

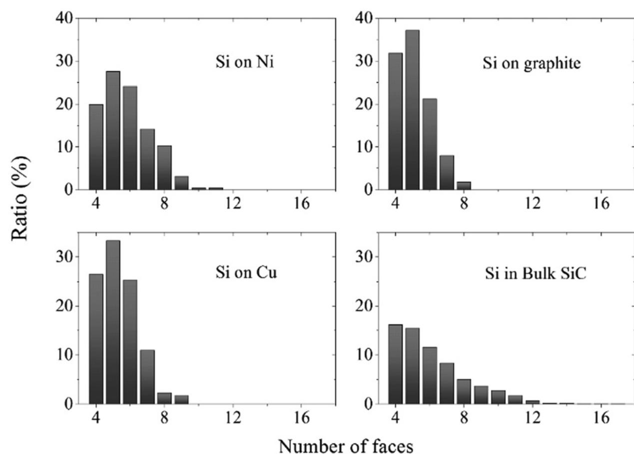

Fig. 9 Distribution of Voronoi polyhedra by the number of faces built for Si atoms of SiC films obtained on nickel, graphite, and copper substrate, in comparison with the corresponding distribution for the silicon subsystem of the 4H-SiC bulk phase of silicon carbide modification.

Presented in Fig. 11 the m distributions for the Si subsystem in SiC films on Ni, Cu and graphite substrates, as well as in the bulk phase of SiC have even less variability compared to the corresponding m-distributions for the C subsystem. In this case, for all the considered systems, the maximum of m distribution falls on m_m = 4. For all m distributions related to films, the fraction of triangular faces exceed the fraction of pentagonal faces. However, in the case of the bulk SiC phase, on the contrary, the fraction of pentagonal faces (37.4%) turns out to be commensurate with the fraction of quadrangular faces (38.3%) and exceeds the fraction of triangular faces by a factor of 3.3. The clear predominance of quadrangular faces for the C and Si subsystems in the films obtained on Ni, Cu, and graphite substrates indicates a significant crystallinity structure of these films.

In order to determine the film with the most degree of crystallinity, the angular distributions (φ distributions) of the nearest geometric neighbors are considered. Geometric neighbors are determined by their formation of VP faces. The angle φ

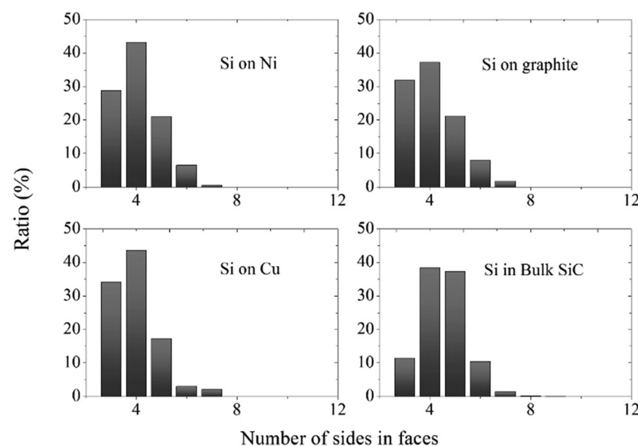

Fig. 11 The distribution of the faces of the Voronoi polyhedrons by the number of sides for the Si subsystem of SiC films obtained on nickel, graphite, and copper substrate, in comparison with the corresponding distribution for the silicon subsystem of the 4H-SiC bulk phase of the modification of silicon carbide.

has its vertex at the center VP, and the sides of this angle pass through a pair of geometric neighbors. When constructing φ distributions, all constructed VPs and all pairs of neighbors for each VP are considered. Angular distributions of the nearest geometric neighbors for the C and Si subsystems in SiC-film obtained on three types of substrates (Ni, Cu, graphite) and for the entire SiC flat structure (when both Si and C atoms were taken into account and no size difference was made) formed on these substrates are shown in Fig. 12. The pronounced peaks in the angular distribution reflect the crystallinity of the packing, *i.e.* the higher peaks intensity corresponds to the more regular (crystalline) system.[44,45] Based on the number and location of peaks, one can approximately predict the type of crystal structure. For all constructing angular distributions, the limiting angle was $\varphi = 180^\circ$ (all three atoms forming angle φ located on the same straight line). The angle $\varphi = 0^\circ$ reflects the same geometric situation as the angle $\varphi = 180^\circ$. In other words, when constructing φ distributions, no distinction is made between positive and negative values of the angle φ. Thereby, when constructing φ distributions, the following cases of mutual arrangement of atoms arise: when three equidistant neighbors are formed in the planar case, an angle $\varphi = 120^\circ$ is created. When 4 neighbors are evenly spaced on the plane around the center, angles $\varphi = 90^\circ$ and 180° can be formed. In the case when an equilateral hexagonal cell is formed around the central atom, the angles $\varphi = 60^\circ$, 120° and 180° can be formed. Indeed,

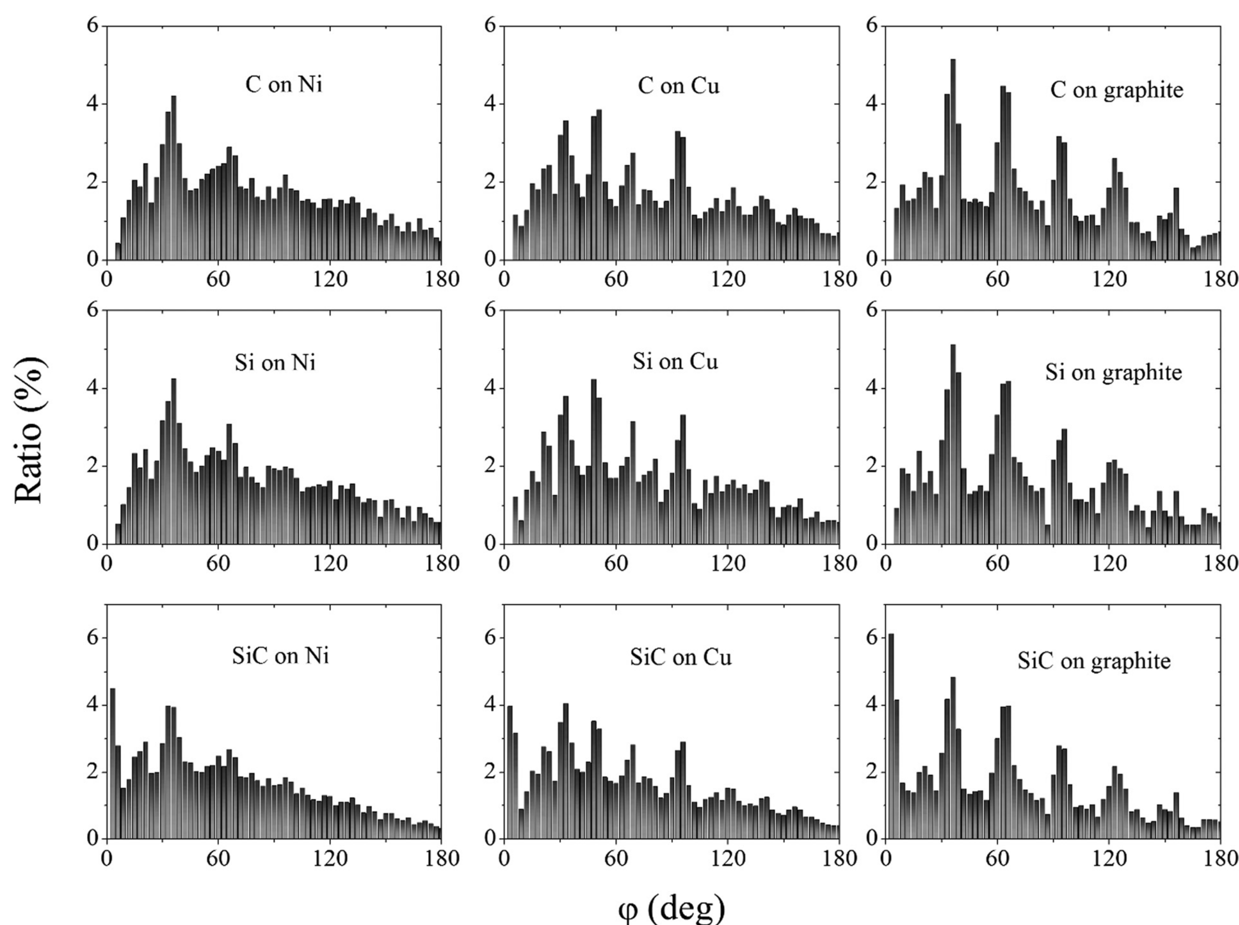

Fig. 12 The angular distribution of nearest geometric neighbors for C and Si subsystems of silicon carbide films and SiC systems as a whole, obtained on Ni, Cu, and graphite substrates.

 This journal is © the Owner Societies 2023

many such nearest neighbors are found if both C and Si atoms are taken into account. For simplicity, we do not take into account differences in the sizes of these atoms. The most regular placement of peaks is observed in the φ distribution of SiC on graphite. In this case, the pronounced peaks correspond approximately to the angles 0° (180°), 30°, 60°, 90°, 120° and 150°. From this list, only the angles of 30° and 150° do not describe the simplest packings of atoms on the plane. However, they can be obtained as linear combinations of standard angles. Both for individual subsystems (Si and C) and for the whole system (SiC), the largest number of high-intensity peaks is formed when the SiC film is located on the graphite, and the least intense peaks are observed in the φ distribution of the SiC film on the nickel substrate. In this sense, the angular distributions for a silicon carbide film and Si, C subsystems on a copper substrate occupy an intermediate position between films on Ni and graphite. Thus, a denser SiC film is immediately formed on graphite, which has the highest degree of crystallinity compared to similar films on metal substrates.

The quality of the film is determined not only by the perfection of its structure, but also by the internal stresses present in the film. The stresses acting in the plane of the SiC film, located on Ni, Cu and graphite substrates, as a result of the application of forces directed along the axes *ox*, *oy* and *oz* (perpendicular to the plane), are shown in Fig. 13. The sign of each local stress is determined by the direction of the resulting force acting on a given area. Unlike macroscopic stress, the sign of local stress does not determine the type of deformation, *i.e.* compression or tension. Therefore, for our estimates, the absolute value of the local stress is important, and not its sign. As can be seen from the figure, the most significant stresses σ_{zx}, σ_{zy}, and σ_{zz} are formed in the SiC film obtained on a copper substrate. Moreover, the local stress σ_{zx}, obtained due to the force acting (along the plane) in the *ox* direction, exceeds the stress σ_{zz} formed due to the action of the force in the perpendicular direction (along *oz*). The considered stresses existing in the SiC film obtained on Ni and graphite are significantly less than the stresses in the film on copper. The internal stresses arising in SiC films formed on Ni and graphite are quite close.

High local stresses do not yet mean high average stresses in the SiC film, since the change in stresses in the film when moving along the *ox* axis has an alternating character. The averaged stress can be computed by integrating the in-plane stress $\sigma_{\alpha\beta}$ at length L of the film. Table 1 shows the stresses applied to the entire SiC film when it is on nickel, copper and graphite substrates. It can be seen that the average stresses related to the entire SiC film are small even in the film located on the copper substrate. Nevertheless, $\bar{\sigma}_{zx}$ in a film on a Cu substrate is at least an order of magnitude greater than similar average stresses obtained on other substrates. Also, a higher absolute value $\bar{\sigma}_{zz}$ of stress observes in SiC film on a copper substrate.

It is of interest to evaluate the effect of each of the considered substrates on the stresses that appear in the SiC film deposited on them.

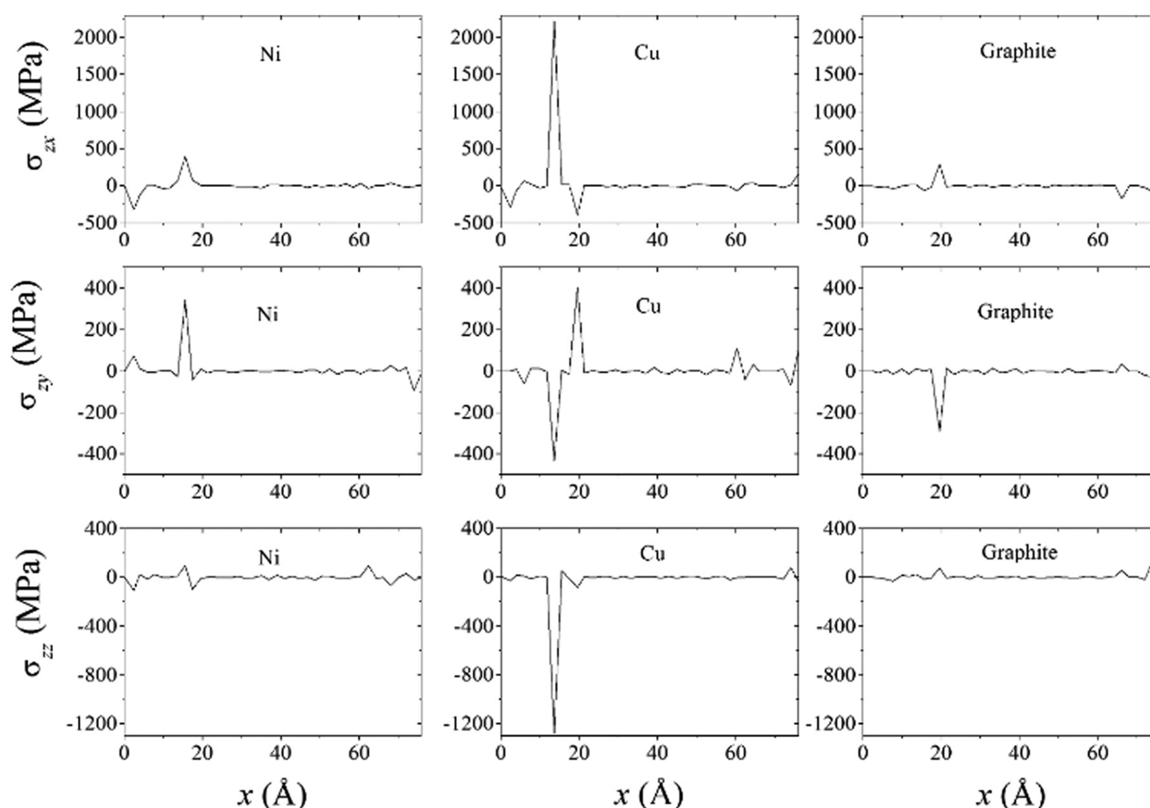

Fig. 13 Stresses acting in the plane of the SiC film obtained on nickel, copper and graphite substrate.

Table 1 Stresses averaged over the entire SiC film acting in its plane

	Substrate material		
Average stress (MPa)	Ni	Cu	Graphite
$\bar{\sigma}_{zx}$	1.58	43.39	−2.54
$\bar{\sigma}_{zy}$	8.19	1.55	−7.18
$\bar{\sigma}_{zz}$	−1.38	−31.90	6.09

Fig. 14 shows the stresses that are transferred from the respective substrate to the SiC film deposited on it. In all cases, these stresses are very small, which, as a rule, are 2–3 orders of magnitude lower than the internal local stresses existing in the films themselves. It should be noted that the most significant stresses transferred from the substrate to the SiC film are the stresses σ'_{zz} determined by the force acting in the direction perpendicular to the film plane. The largest local stresses σ'_{zz} are transferred to the film from Cu and the graphite substrate. These stresses are approximately 4.1 times higher than the corresponding stress transmitted from the Ni substrate. Thus, the nickel substrate has a minimal effect on the formation of internal stresses in the SiC film in comparison with copper and graphite substrates.

4. Discussion

Calculations have shown that before a significant part of the area of any of the considered substrates is filled with deposited atoms diffusion of C atoms turns out to be more intense than that of Si atoms. This is most likely due to the influence of the melt on surface diffusion. The fact is that, although in this case diffusion occurs on the surface, it is still carried out in a dense medium created by the melt. In this case, criteria such as the mass and size of atoms come to the fore in determining mobility. The silicon atom is 2.3 times heavier than the carbon atom and 1.5 times larger than it. As a result, moving in a dense medium, C atoms turn out to be more mobile than Si atoms. The situation with the ratio of the mobility of C and Si atoms can change in the absence of a melt. The diffusion of Si and C atoms on a single graphene layer and between graphene sheets was studied in ref. 46. It was shown that Si atoms moved almost freely over graphene and between graphene layers, while C atoms moved more slowly due to higher diffusion barriers. This behavior of C and Si atoms explains the growth of epitaxial graphene on the SiC surface, when Si atoms evaporate during growth. Moreover, Si atoms continue to evaporate even after the formation of surface graphene layers.

Our results in the deposition of SiC films have a theoretical substantiation. If atomic layer deposition (ALD) is achieved during film growth, this means that the deposited substance enters into a self-limiting reaction with the growth surface. Knowing the mechanisms of ALD will allow you to control the growth of the material.[47] However, when there are few film nucleation sites and the diffusion intensity cannot be significantly increased, islands or nanoparticles are formed on the surface instead of a homogeneous film.[48] Film formation is by

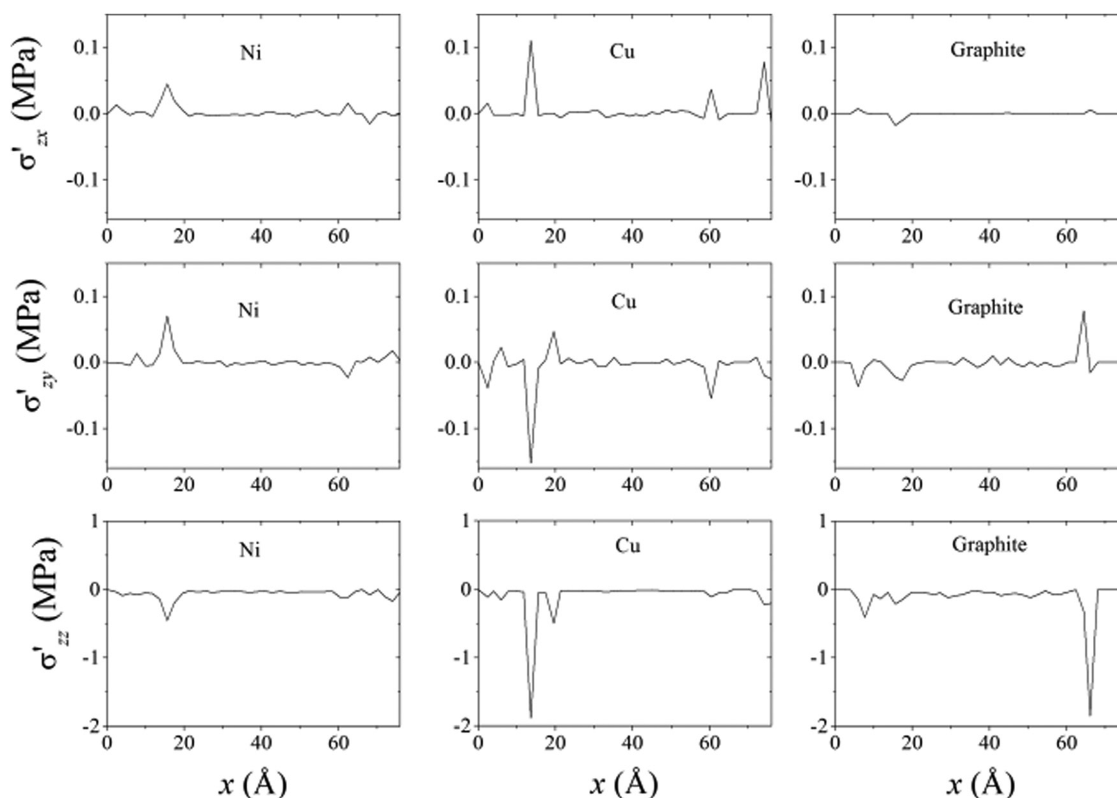

Fig. 14 Stresses propagated on the SiC film as a result of its interaction with nickel, copper and graphite substrate.

 This journal is © the Owner Societies 2023

affected both nucleation and chemisorption. Chemisorption is performed in the form of creating formal chemical bonds between the deposited substance and the substrate, which are necessary to support growth. Since the deposited substance reacts with the growth surface, but not itself, this leads to the self-limiting characteristic of ALD. Chemisorption can lead to the creation of volatile byproducts, those byproducts should readily desorb from the surface and be purged away. As a result, chemisorption becomes essentially irreversible. However, chemisorption can be potentially reversible. This happens when byproducts are not produced or do not desorb.[49] It is generally believed that physical adsorption plays a secondary role in film formation. It acts as an assistant to chemisorption. This is due to the weakness of intermolecular forces between the deposited substance and the substrate, which can cause desorption. In addition, physical adsorption due to van der Waals forces does not have an inherent mechanism for self-limitation.

At the initial stage of growth, the origin of growth centers occurs. Growth begins when a significant number of growth nuclei are formed. The period of accumulations of growth nuclei is commonly called the delay in nucleation. This delay is explained by the absence of chemisorption or its very slow development during this period. Usually the strong nucleation delay occurs on low energy surfaces, but there is almost no nucleation delay on high energy metal surfaces. The nature of the substrate can also significantly affect chemisorption. So, nickel, due to its high surface energy, can have significant dissociative chemisorption, while graphite does not show this. In addition, there is a dependence of chemisorption on the structure of the material, *i.e.* chemisorption can be different on the same material. The adsorption of Si on metal substrates is favorable. In this case, there is an excess of active centers for chemisorption, which contributes to the formation of a monolayer. During the adsorption of Si on graphite, the growth of islands separated by bare substrate. In other words, the island growth mechanism is observed here. The difference in the mechanisms of film formation is due not only to the substrate material, but also to different diffusion over the substrate surface. Diffusion of chemisorbed particles leads to their encounter with previously settled atoms, which leads to the formation of clusters. However, island growth can also occur in a diffusionless regime. This occurs with very slow chemisorption. Surface diffusion of particles can be considered using the localized hopping model.[50] An increase in the surface diffusion increases the rate of aggregation. The growth of islands is observed, for example, during the formation of nanoparticles of noble metals on dielectric substrates.

There is reason to believe that at the final stage of filling the substrate with C and Si atoms, the adhesion of the SiC film to the substrate will decrease. This may be due to the fact that the newly inserted C and Si atoms can slightly shift neighboring atoms and put them in energetically less favorable positions. At the same time, they themselves cannot reach energetically favorable positions. Such an effect was observed during the deposition of alkali metal atoms on the (0001) graphite surface, where the interaction of the two-dimensional metal film with the substrate weakens with an increase in the coverage of graphite with an alkali metal.[51] As a result of the weakening of adhesion to the substrate, the C and Si atoms located on it will be more and more alienated from it and transferred to the bulk of the system; bond more strongly with the melt. Blocked by the melt ions, but not completely detached from the substrate, they lose the ability to move significantly. Therefore, the self-diffusion coefficient of atoms deposited on the substrate decreases significantly when a high degree of coverage of the substrate by these atoms is achieved.

A detailed structural analysis performed using the construction of Voronoi polyhedra made it possible to establish that the predominantly single-layer SIC films obtained by us are not completely amorphous, but have a certain degree of crystallinity.

Crystallinity is more related to the film obtained on graphite, and in the film on a nickel substrate, it is most weakly expressed. Crystallinity is formed due to ''patterns'' formed due to the stacking of fragments of Si and C atoms, represented as triangles, quadrangles and hexagons. Due to the empty gaps in the stacking of the deposited atoms and the difference in the heights of their location above the substrate, in the mutual arrangement of atoms, angles appear that are close to 30° and 150°. In this case, the polyhedra are three-dimensional bodies, not flat figures.

The SiC films we obtained on a copper substrate have a high internal stress σ_{zx} (up to 2.2 GPa) and probably exist only due to the presence of the substrate. At the same time, in SiC films deposited on nickel and graphite substrates, there is a moderate residual stress σ_{zy} (up to 345 MPa), which, like the stress in a film on a Cu substrate, should be removed by annealing.

The difference in calculated internal stresses for films on metal and graphite substrates can be associated with different thermal conductivity properties of materials. The coefficient of linear expansion α of graphite is 2.5 times greater, and similar characteristics of Cu and Ni are two orders of magnitude greater than α for SiC.[52–54] It can be assumed that the thermal stresses observed at room temperature in the SiC film obtained on graphite will be lower than in the case of using metal (Cu and Ni) substrates.

Internal stresses remain in the film after its production and can even increase under the influence of the external environment. In ref. 55, the change in the residual stress in films of amorphous silicon carbide (a-SiC:H) exposed to air and moisture was studied. The films were obtained by the plasma enhanced chemical vapor deposition method. The low temperature of film deposition (423 K) contributed to the accumulation of internal stresses, the value of which, after 28 days of exposure, could reach 420 MPa. Predominantly amorphous SiC films obtained by magnetron sputtering have a high internal compressive stress, which turns into a tensile stress after annealing at a temperature $T > 773$ K.[56] The films may contain microcracks after annealing. However, they are able to withstand compressive stresses up to 1.2 GPa as well as tensile stresses up to 0.6 GPa.

The stress problem in thin films is well known. However, there are still no clear ideas on how to deal with this, how to

adapt and how to control the voltage when using thin films in many areas. Almost every method of film synthesis creates this problem. Voltage development during film synthesis occurs in the physical vapor deposition, chemical vapor deposition, plasma chemical vapor deposition and other methods. The appearance of stresses in films is the result of interrelated processes and various factors. In the case when there is a huge amount of heterogeneous stress data, it is extremely difficult to present a single picture and create a comprehensive model of the occurrence of stresses. The internal stress may depend on grain size, film growth rate, and conditions for energy release. Strategies for reducing excessive voltage levels depend on the type of synthesis and many other factors. Among the means of combating stress in films, there may be ways leading to stress relaxation and compensation. In addition, the control of film growth conditions is being developed and improved.

It is known that a tensile stress can exist in a metal film at the interface with the substrate.[57] The reason for this is the mismatch between the lattice periods of the crystalline film and the substrate. In the systems we are studying, the Si–C bonds existing in the film are much stronger than the bonds in the metal substrate. Therefore, significantly higher stresses appear in films on Ni and Cu than in these metal substrates. In other words, significant local stresses are formed in the SiC films themselves rather than being transferred to the film through the substrate.

The mechanical properties of the SiC film are largely determined by the density of Si–C bonds.[58] In particular, hardness and modulus of elasticity have an increasing linear dependence on the number of Si–C bonds. Therefore, it is important to optimize the growth conditions of the SiC film in order to obtain the highest possible density of Si–C bonds. The maximum density of Si–C bonds is achieved during the formation of stoichiometric silicon carbide.[59] Not all methods for the synthesis of silicon carbide films can guarantee the obtaining of a homogeneous structure of this two-dimensional material. So, for example, SiC films, obtained by pulsed laser deposition on Si (100) were a mixture of silicon dioxide and silicon carbide.[58]

5. Conclusion

In this study, we showed the fundamental possibility of obtaining SiC films by electrolytic deposition from a KCl–KF–KI ternary melt. Regardless of the substrate type, the surface diffusion of C atoms is higher than the mobility of Si atoms. It has been established that during deposition on a graphite surface, the growth of the SiC film occurs from a small number of active centers, while in the case of metallic substrates take place predominantly multi-center layer by layer SiC growth. The silicon carbide film obtained on graphite has a higher density and a shorter Si–C bond length than a film deposited on metal surfaces. The substrate material it also effects on the crystallinity degree of the SiC film: the film on the graphite has a higher crystallinity than on nickel and copper substrates. The films obtained on graphite and nickel are characterized by lower average stresses than a film deposited on a copper substrate. The strongest local stresses are found in the SiC film obtained on a copper substrate. The nickel substrate makes a smaller contribution than the copper and graphite substrates to the local stresses existing in the film. Partial stress relief in SiC films obtained by the electrolytic method can be carried out using annealing without removing the film from the substrate.

Future research may be aimed at determining the optimal composition of the electrolyte used to deposit the SiC film. The method of electrolytic production of coatings of various morphology and composition can be applied in the case of geometrically complex surfaces.

Author contributions

Alexander Y. Galashev: conceptualization, writing – review and editing, formal analysis, project administration. Ksenia A. Abramova: conceptualization, methodology, software, writing – original draft, formal analysis.

Conflicts of interest

There are no conflicts to declare.

Acknowledgements

This work is executed in the frame of the scientific theme of Institute of High-Temperature Electrochemistry UB RAS, number FUME-2022-0005, registration number 122020100205-5.

Notes and references

1 *Physics and Technology of Silicon Carbide Devices*, ed. M. A. Fraga, R. Pessoa, M. Massi, H. S. Maciel, Y. Hijikata, Intech, Japan, 2012, pp. 313–336.
2 Md Habibur, E. H. Chowdhury, D. A. Redwan, S. Mitra and S. Hong, *Phys. Chem. Chem. Phys.*, 2021, **23**, 5244.
3 A. S. Jannatulislam, Md Sherajul Islam, N. Ferdous, J. Park and A. Hashimoto, *Phys. Chem. Chem. Phys.*, 2020, **22**, 13592.
4 C. Raynaud, D. Tournier, H. Morel and D. Planson, *Diam. Relat. Mater.*, 2010, **19**, 1.
5 J. H. Scheiffarth, B. J. Wagner, K. Brennfleck and W. Huettner, *Surf. Coat. Technol.*, 1992, **54**, 13.
6 S. Santavirta, M. Takagi, L. Nordsletten, A. Anttila, R. Lappalainen and Y. T. Konttinen, *Arch. Orthop. Traum. Surg.*, 1998, **118**, 89.
7 J. K. Seo, K. H. Ko, W. S. Choi, M. Park, J. H. Lee and J. S. Yi, *J. Cryst. Growth.*, 2011, **326**, 183.
8 M. D. Stamate, *Appl. Surf. Sci.*, 2001, **172**, 47.
9 T. Stapinski, B. Swatowska, S. Kluska and E. Walasek, *Appl. Surf. Sci.*, 2004, **238**, 367.
10 M. D. Stamate, I. Lazar and G. Lazar, *J. Non-Cryst. Solids*, 2008, **354**, 61.
11 M. J. Ledoux and C. P. Huu, *CATTECH*, 2001, **5**, 226.

This journal is © the Owner Societies 2023

12 G. M. Wells, S. Palmer, F. Cerrina, A. Purdes and B. Gnade, *J. Vac. Sci. Technol., B*, 1990, **8**, 1575.
13 C. P. Huelmo, M. G. Menezes, R. B. Capaz and P. A. Denis, *Phys. Chem. Chem. Phys.*, 2020, **22**, 16096.
14 M. Büttner, P. Choudhury, J. K. Johnson and J. T. Yates Jr, *Carbon*, 2011, **49**, 3937–3952.
15 T. Hu, D. Ma, Q. Fang, P. Zhang, X. Liu, R. Wei, Y. Pan, K. Xuand and F. Ma, *Carbon*, 2019, **146**, 313–319.
16 A. M. Ouadfel, A. Keffous, A. Khelouf, A. Cheriet, C. Yaddaden, N. Gabouze, M. Kechouane, Y. Belkacem, A. Boukezzata, S. Kaci, L. Talbi, Y. Ouadah, I. Bozetine, B. Rezgui, L. Guerbous, H. Menari, B. Mahmoudi and I. Menous, *Opt. Mater.*, 2017, **65**, 117.
17 V. Tiron, E.-L. Ursu, D. Cristea, G. Bulai, G. Stoian, T. Matei and I.-L. Velicu, *Nanomater.*, 2022, **12**, 512.
18 S. I. Molina, F. M. Morales and D. Araújo, *Mater. Sci. Eng. B*, 2001, **80**(1–3), 342.
19 M. N. Grigoryev, T. N. Myasoedova and T. S. Mikhailova, *IOP Conf. Series: J. Phys.: Conf. Series.*, 2018, **1124**, 081043.
20 A. Isakov, A. Khudorozhkova, A. Redkin and Y. Zaikov, *J. Rheol.*, 2021, **65**, 171.
21 M. V. Laptev, A. V. Isakov, O. V. Grishenkova, A. S. Vorob'ev, A. O. Khudorozhkova, L. A. Akashev and Y. P. Zaikov, *J. Electrochem. Soc.*, 2020, **167**, 042506.
22 A. Khudorozhkova, A. Isakov, A. Apisarov, A. Redkin and Y. Zaikov, *J. Chem. Eng. Data*, 2020, **65**, 2505.
23 A. O. Khudorozhkova, A. V. Isakov, A. A. Kataev, A. A. Red'kin and Yu. P. Zaikov, *Russ. Metall. (Met.)*, 2020, **8**, 918.
24 A. Isakov, A. Apisarov, A. O. Khudorozhkova, M. Laptev and Yu. P. Zaikov, *J. Phys. Conf. Series.*, 2018, **1134**, 012021.
25 X. Zou, L. Ji, X. Yang, T. Lim, E. T. Yu and A. J. Bard, *J. Am. Chem. Soc.*, 2017, **139**, 16060.
26 G. Opletal, B. Sun, T. C. Petersen, S. P. Russo and A. S. Barnard, *Phys. Chem. Chem. Phys.*, 2019, **21**, 6517.
27 K. A. Ivanichkina, A. Y. Galashev and A. V. Isakov, *Appl. Surf. Sci.*, 2021, **561**, 149959.
28 A. Y. Galashev, *J. Phys.: Condens. Matter*, 2021, **33**(49), 495103.
29 A. Parretta, G. Giunta, E. Cappelli, A. Adoncecchi and V. Vittori, *MRS Online Proc. Libr.*, 1989, **168**, 227.
30 S. E. Saddow, *Silicon Carbide Biotechnology: A Biocompatible Semiconductor for Advanced Biomedical Devices and Applications*, Elsevier, Amsterdam, 2nd edn, 2016, ISBN 978-0-12-385906-8.
31 P. Leidinger and S. Gunther, *J. Phys. Chem. C*, 2021, **125**, 12663.
32 A. Istratov, C. Flink, H. Hieslmair, S. McHugo and E. Weber, *Mater. Sci. Eng. B*, 2000, **72**, 99.
33 V. V. Kidalov, S. A. Kukushkin, A. V. Osipov, A. V. Redkov, A. S. Grashchenko, I. P. Soshnikov, M. E. Boiko, M. D. Sharkov and A. F. Dyadenchuk, *Mater. Phys. Mech.*, 2018, **36**, 39.
34 H. Loulijat, H. Zerradi, A. Dezairi, S. Ouackit, S. Mizani and F. Rhayt, *Adv. Powder. Tech.*, 2015, **26**, 180.
35 J. Tersoff, *Phys. Rev. B: Condens. Matter Mater. Phys.*, 1994, **49**, 16349.
36 L. Grippo and S. Lucidi, *Math. Program.*, 1997, **78**, 375.
37 A. Y. Galashev and A. S. Vorob'ev, *Materials*, 2022, **15**, 3863.
38 P. Mocci, R. Cardia and G. Cappellini, *IOP Conf. Series: J. Phys.: Conf. Ser.*, 2018, **956**, 012020.
39 A. Y. Galashev and K. A. Ivanichkina, *Phys. Chem. Chem. Phys.*, 2019, **21**, 12310.
40 J. Grundenberg, *Angew. Chem., Int. Ed.*, 2001, **40**(21), 4027.
41 Md. H. Rahman, S. Mitra, M. Motalab and P. Bose, *RSC Adv.*, 2020, **10**, 31318.
42 M. Ishimaru, *Nucl. Instr. Meth. Phys. Res. B*, 2006, **250**, 309.
43 Md Nuruzzaman, M. Ariful Islam, M. Ashraful Alam, M. A. Hadi Shah and A. M. M. Tanveer Karim, *Int. J. Eng. Res. Appl.*, 2015, **5**(5), 48.
44 A. E. Galashev and V. P. Skripov, *J. Struct. Chem.*, 1985, **26**, 716.
45 A. E. Galashev and V. P. Skripov, *J. Struct. Chem.*, 1986, **27**, 407.
46 L. Xian and M. Y. Chou, *J. Phys. D: Appl. Phys.*, 2012, **45**(45), 455309.
47 N. E. Richey, C. de Paula and S. F. Rent, *J. Chem. Phys.*, 2020, **152**, 040902.
48 L. Puurunen and W. Vandervorst, *J. Appl. Phys.*, 2004, **96**, 4878.
49 R. L. Puurunen, *Chem. Vapor Depos.*, 2003, **9**(5), 249.
50 P. Wynblatt and N. A. Gjostein, *Prog. Solid State Chem.*, 1975, **9**, 21.
51 K. Rytkonen, J. Akola and M. Manninen, *Phys. Rev. B: Condens. Matter Mater. Phys.*, 2007, **75**(7), 075401.
52 T. Middelmann, A. Walkov, G. Bartl and R. Schödel, *Phys. Rev. B: Condens. Matter Mater. Phys.*, 2015, **92**, 174113.
53 Y. Wang, Z. Chen and S. Yu, *J. Mater. Res. Technol.*, 2016, **5**, 170.
54 F. C. Nix and D. MacNair, *Phys. Rev.*, 1941, **60**, 597.
55 F. Deku, S. Mohammed, A. Joshi-Imre, J. Maeng, V. Danda, T. J. Gardner and S. F. Cogan, *J. Biomed. Mater. Res. B Appl. Biomater.*, 2019, **107**(5), 1654.
56 J. H. Jou, L. Hsu, S. Yet and T. Shyy, *Thin Solid Films*, 1991, **201**(1), 69.
57 G. C. A. M. Janssen, *Thin Solid Films*, 2007, **515**(17), 6654.
58 M. Oujja, K. Tabakkouht, M. Sanz, E. Rebollar, M. Sánchez-Arenillas, J. F. Marco, M. Castillejo and R. de Nalda, *Appl. Phys. A: Mater. Sci. Process.*, 2022, **128**, 375.
59 A.-I. Elkhalfi, E. Ech-chamikh, Y. Ijdiyaou, M. A. Azizan, A. Essafti, L. Nkhaili and A. Outzourhit, *Spectrosc. Lett.*, 2014, **47**(5), 392.

This journal is © the Owner Societies 2023